AIChE

Numerical Simulation of the Marangoni Effect on Transient Mass Transfer from Single Moving Deformable Drops

Jianfeng Wang
School of Chemical Engineering and Energy, Zhengzhou University, Zhengzhou 450052, China

Key Laboratory of Green Process and Engineering, Institute of Process Engineering, Chinese Academy of Sciences, Beijing 100190, China

National Engineering Laboratory for Hydrometallurgical Cleaner Production Technology, Institute of Process Engineering, Chinese Academy of Sciences, Beijing 100190, China

Zhihui Wang, Ping Lu, Chao Yang, and Zai-Sha Mao
Key Laboratory of Green Process and Engineering, Institute of Process Engineering, Chinese Academy of Sciences, Beijing 100190, China
National Engineering Laboratory for Hydrometallurgical Cleaner Production Technology, Institute of Process Engineering, Chinese Academy of Sciences, Beijing 100190, China

DOI 10.1002/aic.12494
Published online January 19, 2011 in Wiley Online Library (wileyonlinelibrary.com).

A level set approach was adopted in numerical simulation of interphase mass transfer from a deformable drop moving in a continuous immiscible liquid, and the simulation results on Marangoni effect were presented with respect to three experimental runs in the methyl isobutyl ketone–acetic acid–water system. Experiments showed that when the solute concentration was sufficiently high, the Marangoni effect would occur with the interphase mass transfer enhanced. Numerical results indicated that the mass-transfer coefficient with Marangoni effect was larger than that without Marangoni effect and stronger Marangoni effect made the drop deform more easily. The predictions were qualitatively in accord with the experimental data. Numerical simulation revealed well the transient flow structure of Marangoni effect. © 2011 American Institute of Chemical Engineers *AIChE J,* 57: 2670–2683, 2011
Keywords: drop, level set approach, Marangoni effect, numerical simulation, MIBK–acetic acid–water system

Introduction

It is well known that many industrial processes in chemical engineering, material engineering, power engineering, and other fields are driven by temperature and concentration gradients, which affect significantly the mass/heat transfer rates. If the concentration gradient induces tangential flow at the fluid–fluid interface (the so-called Marangoni convection), the hydrodynamic instability of two-phase flow and therewith the change in the rate of interphase mass transfer may arise. Although the phenomenon of interfacial Marangoni convection has been known for over 150 years, only in recent years increasing interest in this type of instability becomes more striking due to the changing point of view of chemical engineers, who shift their interest gradually from the traditional macroscopic approach to a more mechanismic

Correspondence concerning this article should be addressed to C. Yang at chaoyang@home.ipe.ac.cn.

comprehension of the different transport phenomena taking place at phase boundaries.

The Marangoni convection driven by surface-tension gradient due to concentration or temperature variations along the interface can enhance or suppress the rate of mass or heat transfer. Theoretical studies of the Marangoni effect were mainly based on the linear or nonlinear theory of hydrodynamic instability. A simplified mathematical model from the linear instability theory was first presented by Sternling and Scriven,[1] who predicted the induction of roll cells at the interface, found that the occurrence of Marangoni convection was affected by the direction of mass transfer, concentration level, viscosities, diffusivities and the sensitivity of interfacial tension, and proposed a basic criterion. Pearson[2] first studied thermocapillary convection by a linear stability analysis. Brian[3] extended Pearson's result by including the mechanism of the Gibbs adsorption. Although several approaches have been proposed based on the linear theory, the experimental results in supercritical zones still cannot be explained. Several nonlinear stability analyses of the Marangoni convection were focused on predicting the occurrence of the flow pattern structure and its evolution. Scanlon and Segal[4] first studied the cellular convection driven by surface tension in a semi-infinite liquid layer, and then a case of finite depth was considered by Cloot and Lebon.[5] Golovin et al.'s nonlinear evolution equation was applied in a more realistic system containing a thermally insulated two-layer gas–liquid system with deformable interface.[6] Bragard et al.[7] considered the effect of solute on the Marangoni convection resulting from the mass transfer through the gas–liquid upper surface of a thin liquid layer, and found that hexagonal convection structures are more stable than rectilinear roll cells.

The Marangoni convection accompanied by mass transfer and heat transfer has also been studied extensively using different computational fluid dynamics methods. The influence of the Marangoni effect on the growth of single crystals was considered by Okano et al.,[8] Kobayashi et al.,[9] Gałązka and Wilke,[10] Kawaji et al.,[11] and Braescu and Duffar.[12] A series of papers[13–15] addressed the Marangoni flows in the case of a binary mixture for which the surface tension depends on both temperature and solute concentration. The mixed buoyant-Marangoni convection due to the dissolution of a droplet in a liquid–liquid system with a miscibility gap was investigated by Lappa et al.[16] The Marangoni convections in several gas absorption processes were reported.[17–19] The thermocapillary migration of a droplet or a bubble in a nonuniform temperature field was investigated by Bassano.[20]

To authors' best knowledge, only a few numerical simulations of the Marangoni effect induced by interphase mass transfer to/from drops were ever reported.[21–24] However, the results by Mao and Chen[21] and Wang et al.[22] have not been validated by experimental results, and the shape of the drop is presumed to be spherical. Wang et al.[22] relaxed the restriction of the sphericity but the object of the simulation remained quite general. Wegener et al.[24] simulated fluid dynamics and mass transfer in the Marangoni convection dominated toluene/acetone/water system using the commercial CFD-code STAR-CD on an unstructured grid in a spherical coordinate with the assumption that the drop was spherical and the deformation of drop was ignored. However, besides at much small Reynolds numbers, the moving drop is often deformable in real systems and significant shape change may be caused by the Marangoni effect. The numerical simulation and experimental investigation of Marangoni effect induced by mass transfer of a deformable drop is still an interesting open problem to date. The complexities and difficulties in experiment and numerical simulation of the interphase mass transfer mainly come from the nonlinearity of the fluid flow and the coupling between the velocity and concentration fields through the governing equations and boundary conditions imposed on the interface. Therefore, the concentration distribution and the induced flow structure may be quite different from case to case, in addition to the surface deformation making the problem even more formidable.

In recent years, several different methods for solving multiphase flows have been developed including marker and cell method,[25] volume of fluid method,[26] front tracking method,[27] boundary integral method,[28] level set method,[29] etc. Because Osher and Sethian introduced the level set method for modeling interfacial fronts, this method has been applied in many fields due to its advantage of capturing easily the moving and deformable boundary and easy extension to three–dimensional (3-D) cases.

In this study, the mathematical model of the mass transfer-induced Marangoni effect is formulated for deformable drops in transient motion. The concentration field coupled with flow field is numerically simulated using an in-house computer code. The drop surface evolution is modeled by the level set method, in which the interface is represented by the embedded set of the zero level of a scalar function defined in the whole computational domain. Numerical simulation of the Marangoni effect induced by interphase mass transfer from single drops in unsteady motion with a finite degree of deformation in liquid–liquid extraction systems is performed in an Eulerian axisymmetric reference frame. In particular, the numerical results are compared with the experimental data determined in a methyl isobutyl ketone (MIBK) - acetic acid - water system.

Experimental

To provide the necessary parameters for validating the numerical simulation, the mass transfer of a MIBK–acetic acid–water system was experimentally determined. The experiments were conducted as suggested by Li et al.[30]

Experimental setup

As shown in Figure 1, the experimental equipment is similar to Li et al.[30] The contactor is a glass pipe with 50 mm internal diameter and 700 mm height comprising five side taps for fitting the injection nozzles at different heights. The MIBK drops were formed at the needle tip at a constant rate, which was controlled by a precision syringe pump. All drops were separated by at least a distance of 80 mm. According to the number of drops, the volumetric flow rate of MIBK, and the formation time, the volume-equivalent drop size could be calculated. The rising drops were finally trapped in a small inverted funnel, which was fitted in a standard glass tap hole at the contactor top for collecting the drops. The drops were then sucked into the funnel neck promptly to minimize further mass

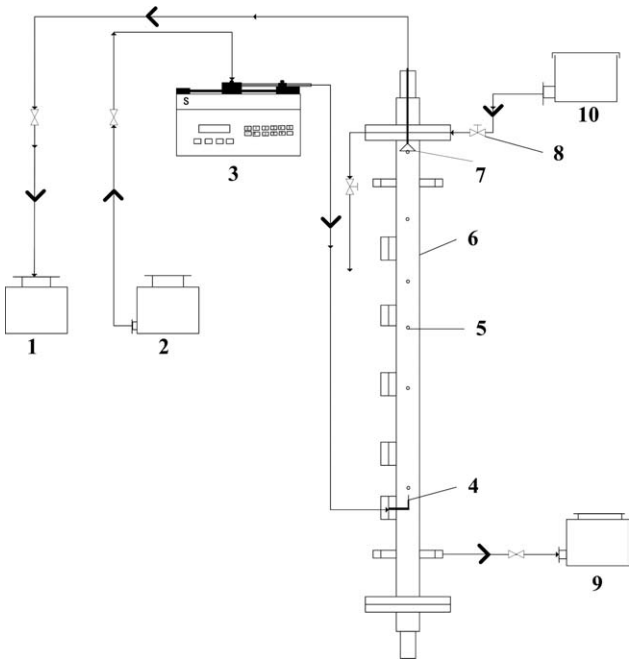

Figure 1. Sketch of experimental setup.

1,2: dispersed phase tank; 3: precision metering pump; 4: nozzle for dispersed phase; 5: moving drop; 6: extractor; 7: funnel; 8: precision adjusting valve; 9,10: continuous phase tank.

transfer. In the experiments, the coalesced phase of first tens of arrived drops was discarded, and when it was removed by suction, care was taken to maintain the coalescence level just at the neck of the funnel.

Preparation of dispersed and continuous phases

The properties of the liquid–liquid systems are summarized in Table 1. The dispersed phase of 1 L of MIBK was mixed with 5 L of continuous phase of deionized water, and then it was fully shaken. The two phases became saturated with each other after a few days and equilibrated. An appropriate amount of the solute (acetic acid) was dissolved separately into the dispersed phase.

The concentration of the solute in the dispersed phase was analyzed, generally more than triplicate times, by titration with 0.1 M NaOH using phenolphthalein as indicator. The relative errors in the experiments are less than 5%.

Procedure

For rising MIBK drops, the collecting funnel was fixed on the top of the contactor. The nozzle tip was inserted into the contactor through a side tap at the desired height. Then, the column was filled with the continuous phase presaturated with MIBK. After the water became stagnant for some time, the precision syringe pump was then started to produce the single drops. In general, the interval between two drops was about 80 mm to minimize the interference of drop wake. The drops collected and coalesced in the funnel were removed by siphon. The dispersed phase of about 5 mL was collected for analyzing the MIBK concentration. The rise of a drop was captured by charge coupled device (CCD) camera, and the transient drop velocity was determined by the post analysis of the recorded drop images. The temperature in all runs controlled in the range of 26.5°C ± 1.5°C.

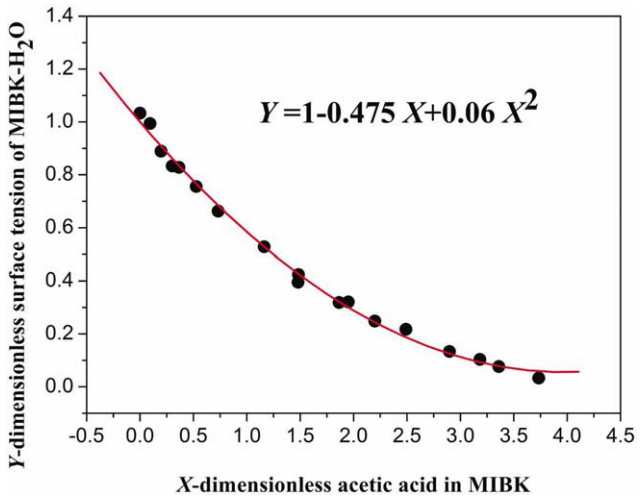

Figure 2. Surface tension of MIBK–acetic acid–water system ($C_{b,0}$ = 7.5%).

[Color figure can be viewed in the online issue, which is available at wileyonlinelibrary.com.]

Mathematical Modeling

The axisymmetric flow of a liquid drop moving under gravity through an immiscible continuous liquid phase is formulated with the following assumptions: (1) the two fluids are viscous, Newtonian and incompressible; (2) the flow is isothermal; (3) the flow field is laminar even if locally disturbed by the Marangoni convection of the inherent 3-D nature; (4) the mass transfer is assumed to have no effect on the physical properties of the system except interfacial tension.

Level set method for two-phase flow

The level set method is used for computing the evolution of an interface Γ that bounds a region Ω in a two-dimensional

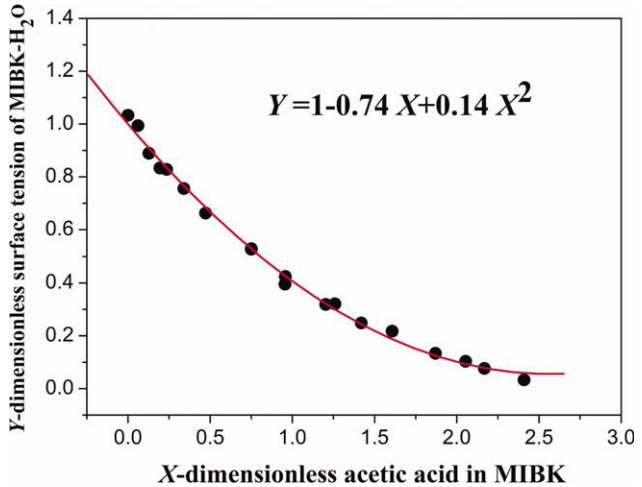

Figure 3. Surface tension of MIBK–acetic acid–water system ($C_{b,0}$ = 12.01%).

[Color figure can be viewed in the online issue, which is available at wileyonlinelibrary.com.]

Table 1. Physical Parameters of the Investigated Liquid–Liquid System with Acetic Acid as Solute

	Continuous phase (water)		Dispersed phase (MIBK)
Run 1			
ρ (kg/m^3)	995.71		827.40
$\mu \times 10^3$ (Pa/s^{-1})	1.069		0.781
$D \times 10^9$ (m^2/s)	1.04		1.43
$\sigma_0 \times 10^3$ (N/m)		9.66	
m		0.70	
R (mm)		0.93	
$C_{b,0}$ (wt %)		7.75	
$C_{c,0}$ (wt %)		0	
Run 2			
ρ (kg/m^3)	995.71		864.60
$\mu \times 10^3$ (Pa/s^{-1})	1.069		0.901
$D \times 10^9$ (m^2/s)	1.04		1.43
$\sigma_0 \times 10^3$ (N/m)		9.66	
m		0.75	
R (mm)		0.90	
$C_{b,0}$ (wt %)		12.01	
$C_{c,0}$ (wt %)		0	
Run 3			
ρ (kg/m^3)	995.71		806.14
$\mu \times 10^3$ (Pa/s^{-1})	1.069		0.63
$D \times 10^9$ (m^2/s)	1.04		1.44
$\sigma_0 \times 10^3$ (N/m)		9.66	
m		0.88	
R (mm)		0.95	
$C_{b,0}$ (wt %)		0.29	
$C_{c,0}$ (wt %)		0	

(2-D) domain. A smooth function $\phi(x,t)$ is defined to represent the interface as the zero set of $\phi(x,t)$, which is positive in one phase, whereas negative in the other phase. Here the level set function ϕ is taken as the normal distance from the interface. Thus, this free boundary problem in principle does not require the direct enforcement of interfacial conditions at the unknown location of the transient interface.

The two-phase flow is governed by the continuity and Navier-Stokes equations:

$$\nabla \cdot \mathbf{u} = 0 \tag{1}$$

$$\rho\left(\frac{\partial \mathbf{u}}{\partial t} + \mathbf{u} \cdot \nabla \mathbf{u}\right) = -\nabla P + \rho g + \nabla \cdot \boldsymbol{\tau} + \mathbf{F}_{\mathrm{Ma}} \tag{2}$$

where τ is the bulk stress tensor defined as

$$\boldsymbol{\tau} = \mu(\nabla \mathbf{u} + (\nabla \mathbf{u})^{\mathbf{T}}) \tag{3}$$

and the source term $\mathbf{F}_{\mathrm{Ma}}$ is the extra volume force generated by the surface-tension gradient that induces the Marangoni effect. The volume force is based on the well-known continuum surface force model,[31] so that the interfacial surface forces can be incorporated as body forces per unit volume in the momentum equations rather than as boundary conditions. The weighted integration method for calculating accurately the surface tension force at the interface nodes is incorporated to suppress the parasitic flow in the level set approach.[32] $\mathbf{F}_{\mathrm{Ma}}$ is exerted on the interface Γ and expressed as

$$\mathbf{F}_{\mathrm{Ma}}(\mathbf{x}) = \mathbf{f}_{\mathrm{s}}(\mathbf{x})\delta(\mathbf{x} - \mathbf{x}_{\mathrm{s}}) \tag{4}$$

where $\mathbf{x}_{\mathrm{s}}$ is the point on Γ, δ is the Dirac delta function, and the surface tension force per unit interfacial area $\mathbf{f}_{\mathrm{s}}$ is given by

$$\mathbf{f}_{\mathrm{s}} = \sigma\kappa\mathbf{n} + \nabla_{\mathrm{s}}\sigma \tag{5}$$

where σ is the surface tension, $\bigtriangledown_{\mathrm{s}}$ is the gradient operator taken along the interface Γ, $\mathbf{n} = -\bigtriangledown\phi/|\bigtriangledown\phi|$ is the unit vector perpendicular to the interface, and κ is the mean curvature of the interface:

$$\kappa = -\nabla \cdot \mathbf{n} \tag{6}$$

The first term in Eq. 5 is a force acting normal to the interface, and the second term is tangential to the interface in the direction of larger values of σ, which may be dependent on temperature or concentration. If only the influence of solute concentration on the surface tension is considered, the following model is assumed:

$$\sigma = \sigma_0(1 + aC_{\mathrm{l}}^{\mathrm{s}} + b(C_{\mathrm{l}}^{\mathrm{s}})^2) \tag{7}$$

where a and b are correlation coefficients, reflecting the influence of solute concentration on the interfacial tension. The correlation is based on the dimensionless solute concentration at the interface to ease the numerical solution of nondimensional governing equations for fluid flow and mass transfer Because $\boldsymbol{C}_{\mathrm{l}}^{\mathrm{s}}$ is based on the initial drop concentration $C_{\mathrm{b},0}$ which varies from run to run, the correlation coefficients a and b have different values, but by dimensional terms they are essentially the same set of experimental data reported by Misek.[33] In particular, $C_{\mathrm{b},0}$ is very low in run 3, the correlation in the range of $0 < C_{\mathrm{l}}^{\mathrm{s}} < 1$ is approximately a flat one with $a = 0$, $b = 0$. For Run 1 in Table 1, $a = -0.475$ and $b = 0.06$; for Run 2 in Table 1, $a = -0.74$ and $b = 0.14$ (Figures 2 and 3).

Considering the concentration change along the surface, Eq. 5 then becomes

$$\mathbf{f}_{\mathrm{s}} = \sigma\kappa\mathbf{n} - \frac{\partial\sigma}{\partial C}(\mathbf{I} - \mathbf{nn}) \cdot \nabla C \tag{8}$$

where $\mathbf{I}$ is the identity tensor and C is the concentration. The last term in Eq. 2 reads

$$\mathbf{F}_{\mathrm{Ma}}(\mathbf{x}) = \quad \sigma\kappa\mathbf{n} - \frac{\partial\sigma}{\partial C}(\mathbf{I} - \mathbf{nn}) \cdot \nabla C \quad \delta(\phi) \tag{9}$$

Thus, Eqs. 1 and 2 coupled with the level set function are written in terms of dimensionless forms in a 2-D moving reference coordinate system fixed on the drop, and the details may be referred to Wang et al.[22] The level set function ϕ and the concentration of solute are advanced with the local velocity at each time step. Maintaining ϕ as a distance function is essential for providing the interface with an invariant width. This problem can be resolved by adopting a reinitialization method proposed by Yang and Mao[34] to keep the solution accurate.

Level set method for interphase mass transfer

The mass transfer of a solute from a drop to the continuous phase is described by

$$\rho\left(\frac{\partial C}{\partial t} + \mathrm{u} \cdot \nabla C\right) = D\nabla^2 C \tag{10}$$

The numerical details of solving the above equation by the level set method are given in Yang and Mao.[35]

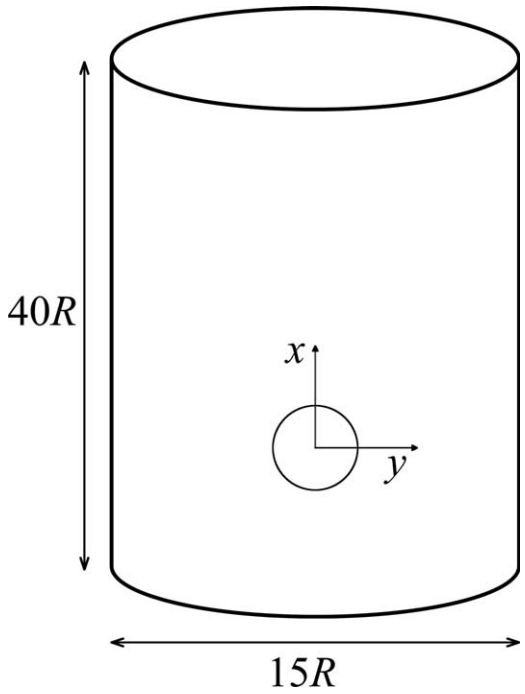

Figure 4. Schematic of computational domain.

The overall mass-transfer coefficient k_{od} is expressed as

$$k_{od} = -\frac{V_d}{S}\frac{1}{t_{out} - t_{in}}\ln\frac{C_2^* - \overline{C}_{2,out}}{C_2^* - \overline{C}_{2,in}} \tag{11}$$

where $\overline{C}_2$ is the average concentration of the drop at any moment, C^* is the concentration in equilibrium with other phase, and V_d and S are the volume and surface area of the drop. The corresponding Sherwood number is

$$Sh_{od} = \frac{2R}{D_1}k_{od} \tag{12}$$

Computational domain and boundary conditions

The coordinate system is fixed at the centroid of the drop. As shown in Figure 4, the computational domain of $40R \times 15R$ (R is the initial radius of a spherical drop,) is found to be sufficient so that the motion of the drop is not affected by the domain boundary. The free slip boundary condition is imposed at the side domain boundaries. The zero-derivative boundary condition is imposed at the inlet and exit of the domain.

The mass-transfer direction is from the drop to the continuous phase (d $\rightarrow$ c). The solute concentration in the continuous phase is assumed to be $C = 0$ at $t = 0$, and the initial concentration in the drop is uniform.

For the present simulation, a quiescent MIBK drop with the concentration $\boldsymbol{C}_b = \boldsymbol{C}_{b,0}$ is released for free rise in water at the instant of $t = 0$ and the mass transfer from the drop to the continuous phase starts at the same time. Other physical parameters at initial moment such as droplet radius, densities of the dispersed and continuous phases, distribution coefficient of a solute, and surface tension for Runs 1–3 are listed in Table 1.

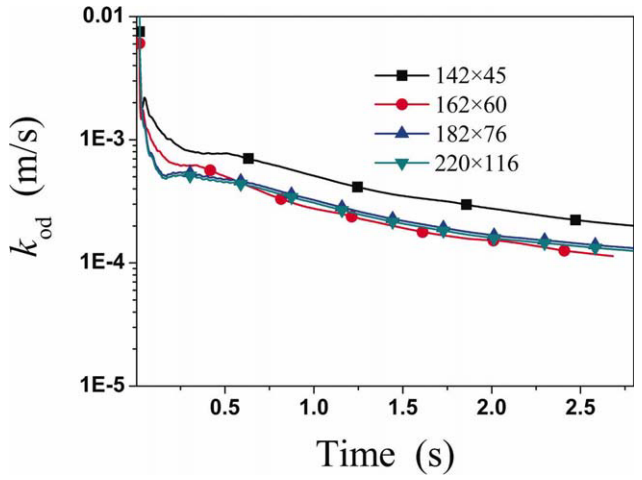

Figure 5. Influence of mesh sizes on the predicted results of overall mass-transfer coefficients ($C_{b,0}$ = 7.5%, physical parameters as listed in Table 1).

[Color figure can be viewed in the online issue, which is available at wileyonlinelibrary.com.]

Computational procedure

The dimensionless parameters in the above equations are the Reynolds, Froude, Weber, and Peclet numbers, respectively:

$$Re = \frac{\rho_1 2RU}{\mu_1}, \quad Fr = \frac{U^2}{2Rg}, \quad We = \frac{2R\rho_1 U^2}{\sigma_0}, \quad Pe = \frac{2RU}{D_1} \tag{13}$$

where ρ_1, μ_1, and D_1 are the density, viscosity, and diffusivity of continuous phase, respectively, and the characteristic velocity is defined as $U = \sqrt{2Rg}$.

The governing equations are discretized by the control volume formulation with the power-law scheme as described by Patankar[36] and solved with the SIMPLEC algorithm[37] on a staggered grid. Pressure, level set function, and concentration are cell centered, and the velocity components are staggered. To ensure the difference accuracy, we use a fifth-order weighted essentially

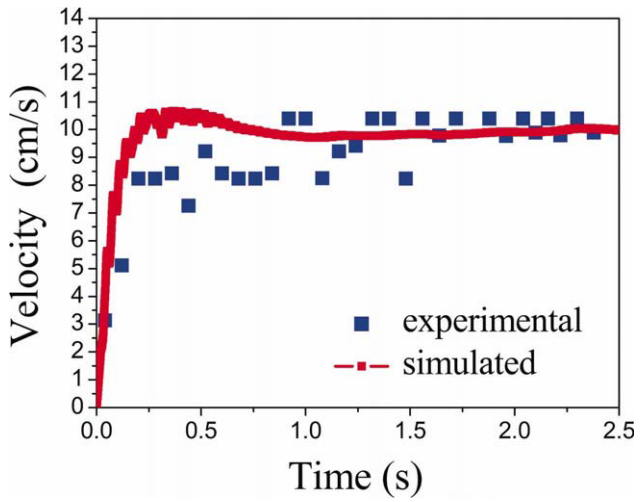

Figure 6. Rising velocity of a MIBK drop in water as a function of time ($C_{b,0}$ = 7.5%).

[Color figure can be viewed in the online issue, which is available at wileyonlinelibrary.com.]

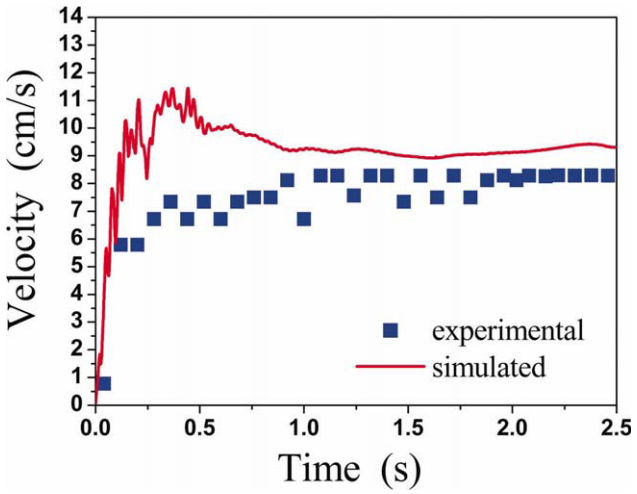

Figure 7. Rising velocity of a MIBK drop in water as a function of time ($C_{b,0}$ = 12.01%).

[Color figure can be viewed in the online issue, which is available at wileyonlinelibrary.com.]

nonoscillatory scheme for the approximation of convective terms in C and ϕ advancing equations, and a third-order total variation diminishing Runge-Kutta scheme is adopted for time discretization of C and ϕ.[34,38,39] The dimensionless time step $\Delta\theta$ is chosen according to Yang and Mao,[34,35] which must satisfy the Courant-Friedrich-Lewy conditions and the restrictions due to gravity, surface tension and viscous terms.

Results and Discussion

The overall mass-transfer coefficient from a drop of MIBK to the continuous phase of water and the velocity of the drop rising in the continuous phase in the MIBK–acetic acid–water system in which the initial concentration of a drop of MIBK is 12.01%, 7.75%, and 0.29% was determined. The reason of choosing the former two concentrations is that at the concentration of 7.75% and 12.01% there

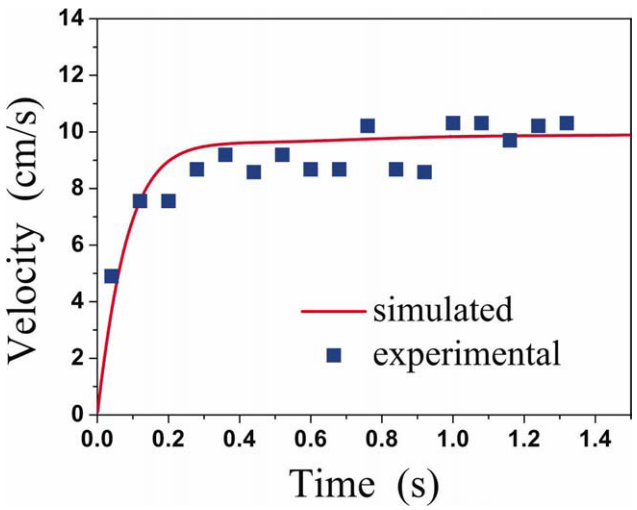

Figure 8. Rising velocity of a MIBK drop in water as a function of time ($C_{b,0}$ = 0.29%).

[Color figure can be viewed in the online issue, which is available at wileyonlinelibrary.com.]

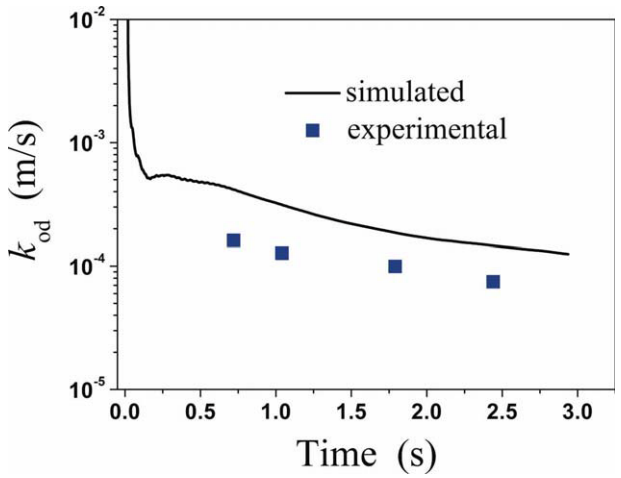

Figure 9. Overall mass-transfer coefficient vs. mass-transfer time ($C_{b,0}$ = 7.5%).

[Color figure can be viewed in the online issue, which is available at wileyonlinelibrary.com.]

was evident Marangoni convection in this system. To compare the influence of Marangoni effect on mass-transfer coefficient and the rising velocity, the mass-transfer rate at the concentration of 0.29% for a MIBK drop without Marangoni convection was also determined. Based on the experimental parameters (as listed in Table 1), the mass transfer from a MIBK drop to the continuous phase was simulated, and the predicted results were compared with the experimental data.

Convergence test

Several nonuniform grids of 142 × 45, 162 × 60, 182 × 76, and 220 × 116 (in axial and radial directions) were tested for comparing the solution of the two-phase flow and interphase mass transfer as a function of time to ensure mesh independence of numerical results. Figure 5 shows the

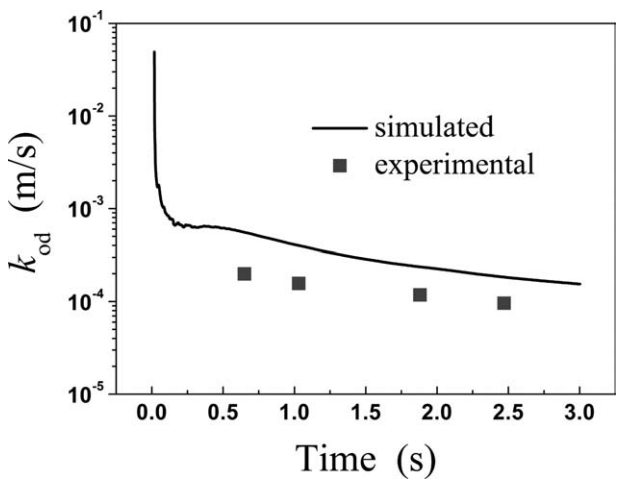

Figure 10. Overall mass-transfer coefficient vs. mass-transfer time ($C_{b,0}$ = 12.01%).

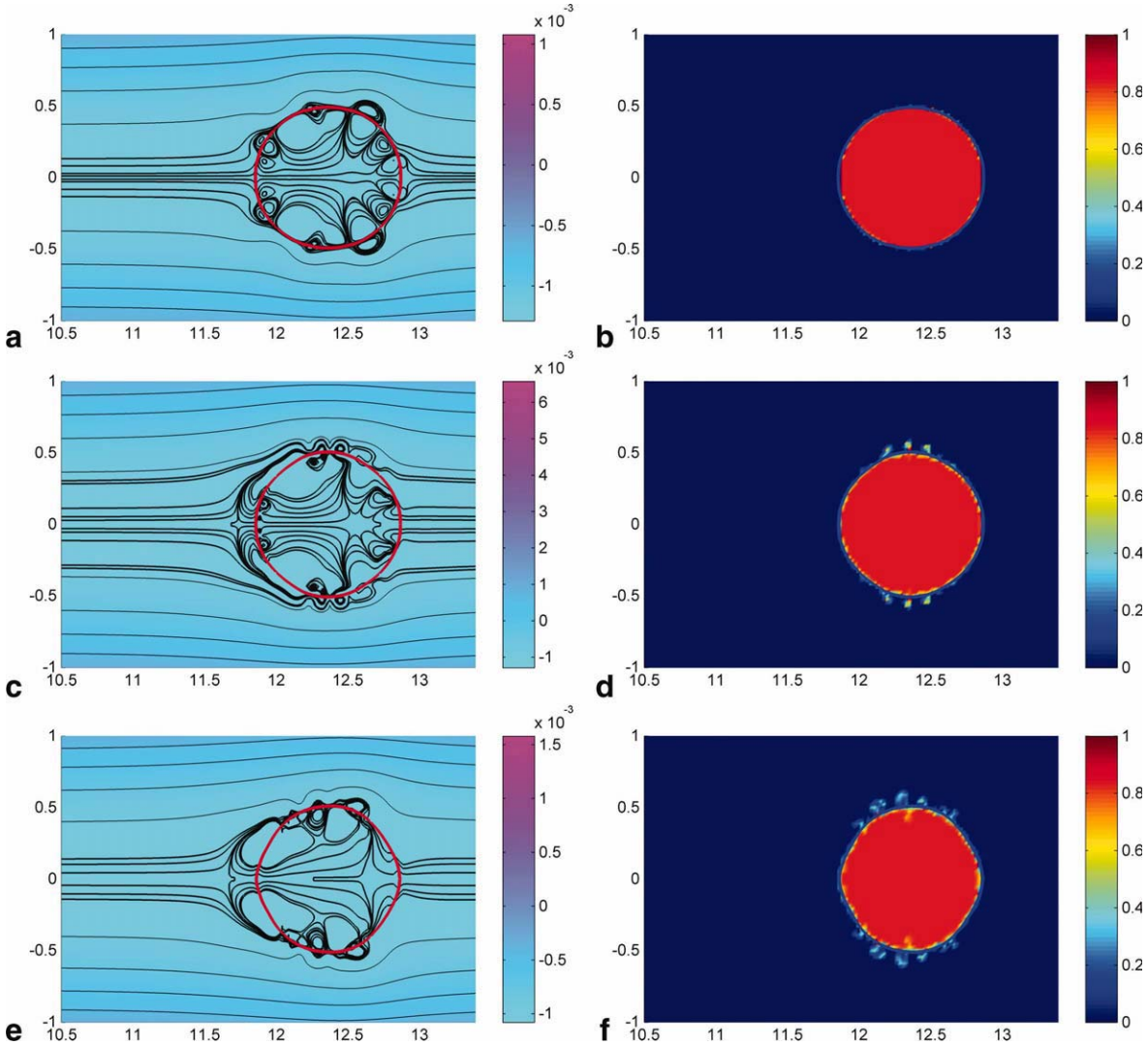

Figure 11. Marangoni effect of a drop changing with time ($C_{b,0}$ = 7.5%).

(a) Contour of stream function (t = 0.001 s), (b) contour of concentration (t = 0.001 s), (c) contour of stream function (t = 0.003 s), (d) contour of concentration (t = 0.003 s), (e) contour of stream function (t = 0.006 s), (f) contour of concentration (t = 0.006 s), (g) contour of stream function (t = 0.008 s), (h) contour of concentration (t = 0.008 s), (i) contour of stream function (t = 0.022 s), (j) contour of concentration (t = 0.022 s), (k) contour of stream function (t = 0.039 s), (l) contour of concentration (t = 0.039 s), (m) contour of stream function (t = 0.430 s), (n) contour of concentration (t = 0.430 s), (o) contour of stream function (t = 0.667 s), (p) contour of concentration (t = 0.667 s), (q) contour of stream function (t = 2.500 s), and (r) contour of concentration (t = 2.500 s). [Color figure can be viewed in the online issue, which is available at wileyonlinelibrary.com.]

influence of mesh size on the overall mass-transfer coefficients. The grid with 182 × 76 nodes is sufficient for spatial computational accuracy, and therefore, adopted for the subsequent simulations.

Drop rising velocity

Figures 6–8 show the experimental and simulation results of the rising velocities of a MIBK drop with different initial solute concentrations in water. The velocity oscillation of the rising drop is noticeable in Figures 6 and 7. This phenomenon is attributed to the Marangoni convection. The instantaneous oscillations of velocity are not easily captured due to the limitation of experimental facilities. The oscillation in drop rising velocities due to the Marangoni effect in the simulation is by principle in agreement with the literature reports on drop shape pulsation. The relative error of the terminal velocity of a rising drop ($C_{b,0}$ = 7.75%) between the experimental and the simulation is less than 4%. The relative error of the terminal velocity for $C_{b,0}$ = 12.09% is below 10%.

The larger the concentration of the drop, the more evident are the Marangoni convection and the oscillation of rising velocity. The oscillation is also more evident in the initial rising stage when the Marangoni convection is stronger due to larger mass-transfer driving force. In the final stage of steady rising, the oscillation of the rising drop becomes invisible gradually as the Marangoni convection dies away with the elapsed time. Figure 8 shows that the velocity of a rising drop of MIBK in water without Marangoni effect increased gradually but monotonously.

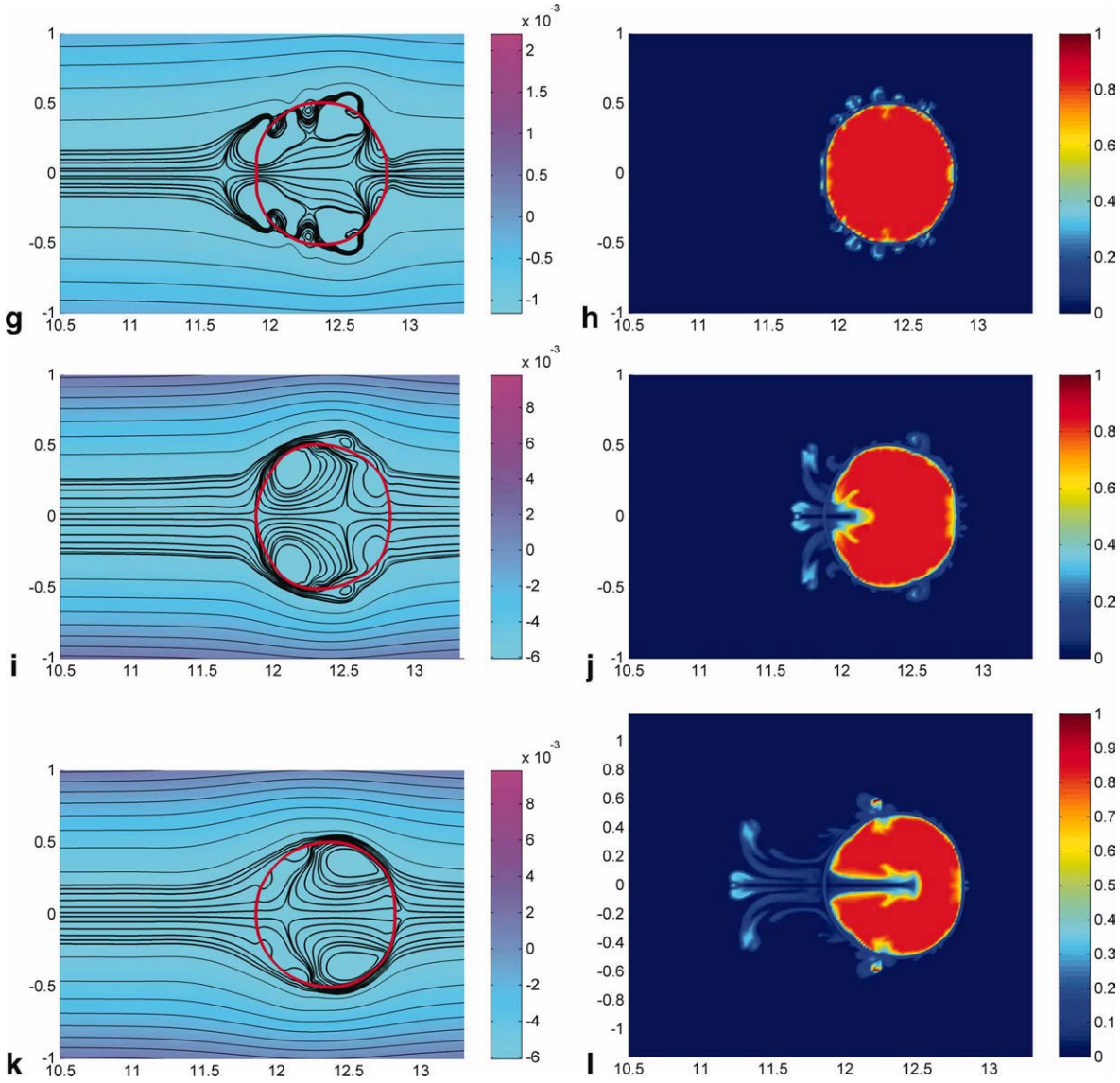

Figure 11. (Continued).

Although the final velocity of a rising drop from numerical simulations is in good agreement with the experimental as shown in Figures 6–8, the vibration of the velocity of a rising drop in numerical simulations is more evident than that in experiments in the initial rising stage, especially when the solute concentration of MIBK drop is large. One of the reasons may be mainly attributed to the numerical scheme. The Marangoni convection is 3-D in nature, but the present model is simplified to a 2-D one. This will result in some nonphysical effect, making the rising velocity of the drop vibrates evidently at the initial rising stage. Another reason is probably that the assumption of the spherical drop and the zero velocity at $t = 0$. In fact, the real drop in the formation and early moving stages was not spherical, and the continuous phase and drop were also in motion with a minor velocity at the moment when a drop was released from the syringe needle.

Mass-transfer coefficient

The exact quantitative prediction of the mass/heat transport rate with the Marangoni effect at present is really a challenge to numerical simulation because of the well-known instability and complexity of the Marangoni effect. Figures 9 and 10 show the overall mass-transfer coefficients with different initial solute concentrations, i.e., 7.75% in Figure 9 and 12.01% in Figure 10, respectively. The experimental measurements are found to accord in the decreasing trend of the numerical results of k_{od}, but the numerical predictions are greater than the experimental data. Bigger diameter and greater deformation of drops in the MIBK–acetic acid–water system cause larger numerical and experimental errors of mass-transfer coefficients than those in the water–succinic acid–butanol system.[40] Another important reason is that the present axisymmetric simulation captured only the Marangoni effect in form of toroidal roll cells, which are easier to

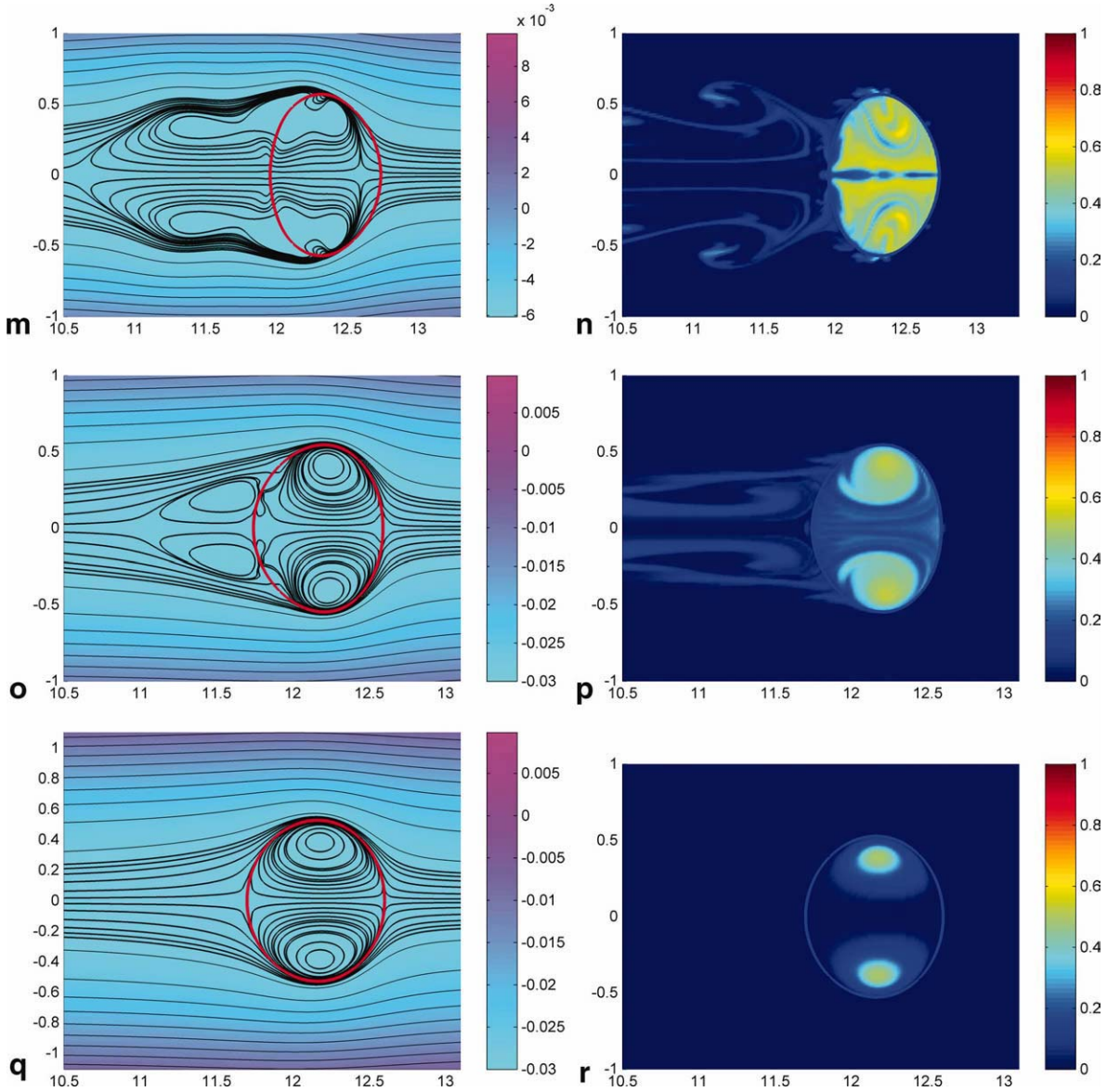

Figure 11. (Continued).

be triggered than the hexagonal convection structure contributing to enhanced interphase mass transfer according to Bragard et al.[7] and Mao et al.[41] Probably, the higher predicted velocities in numerical simulations also result in higher convective intensity, especially in the initial rising stage of the drop, contributing somewhat to higher mass-transfer rate.

Discussion

To understand the influence of the Marangoni effect on the interphase mass transfer, the transient evolutions of stream function and concentration contours for the case of the initial solute concentration of 7.75% in the drop at different times are shown in Figure 11, and for the case of 12.01% in Figure 12, respectively. Figures 11 and 12 show the obvious deformation of a drop at different instants. The transient stream function map changes constantly due to the Marangoni effect. The drop deforms gradually from initially spherical to finally ellipsoidal as an overall trend, but irregular shapes appeared as depicted in Figure 11 and more evidently in Figure 12, indicating that the larger the initial solute concentration in the drop, the more intensive the Marangoni effect. Wegener et al.[24] also observed similar irregular great deformation of the drop in the toluene–water system without mass transfer and Marangoni convection. There are some small eddies of sub-drop dimensions near the interface. These eddies make the interfacial tension change obviously along the interface to bring forth strong local interfacial convection with velocity components perpendicular to the interface and make the interface deform greatly. The deformation of the interface is irregular due to the transient nature of Marangoni effect. Figure 12 shows that the irregular shape of the interface is more evident at the initial stage of the mass transfer, especially at the larger initial concentration of

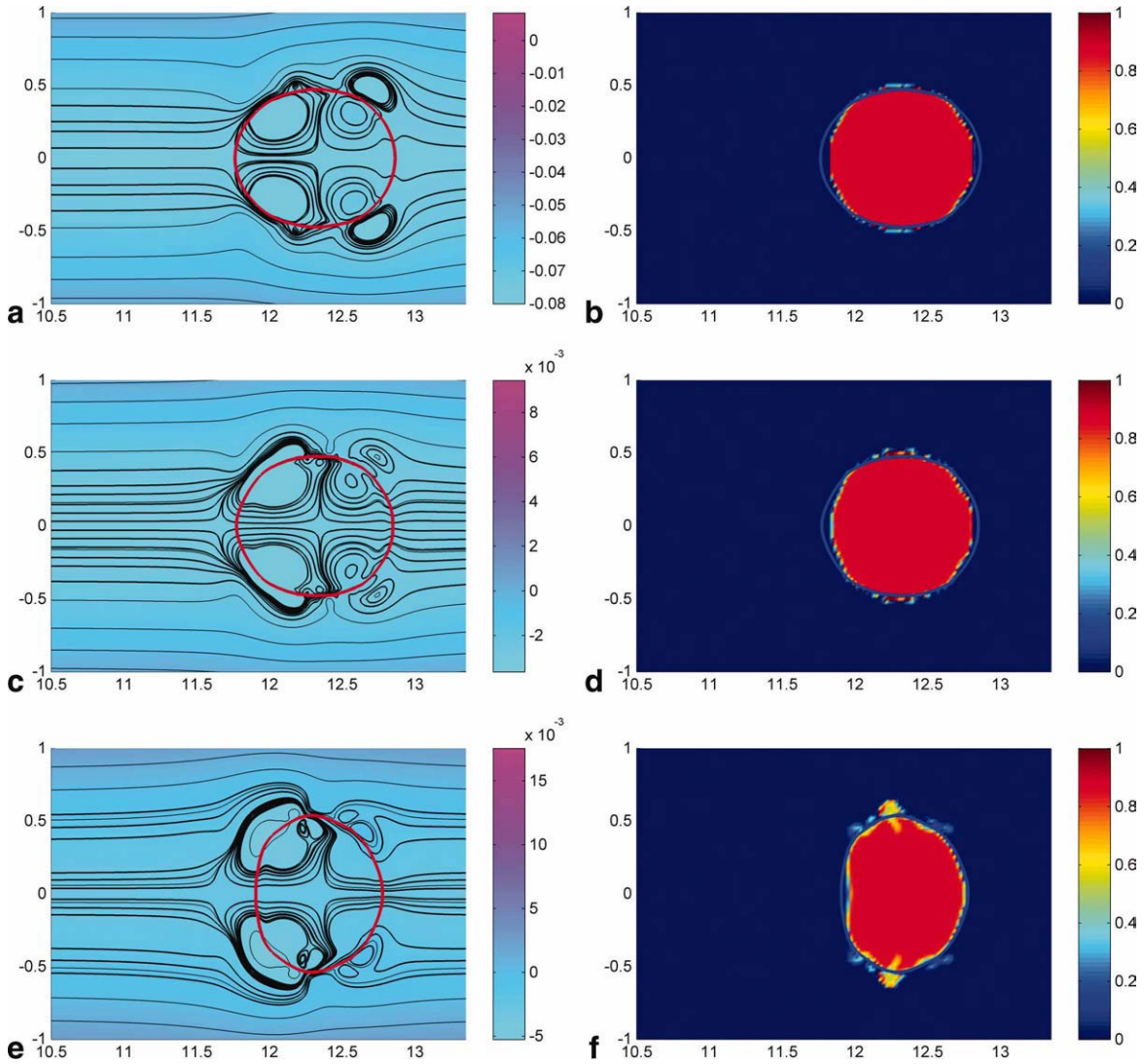

Figure 12. Marangoni effect of a drop changing with time ($C_{b,0}$ = 12.01%).

(a) Contour of stream function ($t = 0.001$ s), (b) contour of concentration function ($t = 0.001$ s), (c) contour of stream function ($t = 0.002$ s), (d) contour of concentration function ($t = 0.002$ s), (e) contour of stream function ($t = 0.005$ s), (f) contour of concentration function ($t = 0.005$ s), (g) contour of stream function ($t = 0.008$ s), (h) contour of concentration function ($t = 0.008$ s), (i) contour of stream function ($t = 0.023$ s), (j) contour of concentration function ($t = 0.023$ s), (k) contour of stream function ($t = 0.039$ s), (l) contour of concentration function ($t = 0.039$ s), (m) contour of stream function ($t = 0.11$ s), (n) contour of concentration function ($t = 0.11$ s), (o) contour of stream function ($t = 0.34$ s), (p) contour of concentration function ($t = 0.34$ s), (q) contour of stream function ($t = 2.5$ s), and (r) contour of concentration function ($t = 2.5$ s). [Color figure can be viewed in the online issue, which is available at wileyonlinelibrary.com.] [Color figure can be viewed in the online issue, which is available at wileyonlinelibrary.com.]

the drop. In all cases, the Marangoni convection vanishes gradually along the mass-transfer time. The shape of the drop is gradually deformed to ellipsoidal one that is similar to the characteristic of steady-state motion. In our experiments, the transient local Marangoni convection near the interface can also be observed qualitatively by CCD.

3 Figure 13 shows the enhancement of the transient Marangoni effect on the mass-transfer coefficient in experiments and numerical simulations for different initial drop concentrations. The mass-transfer coefficient for the case of $C_{b,0} = 12.01\%$ is the largest in the numerical simulation and in the experiment. The predicted change of mass-transfer coefficient is in accord with the trend detected in the experiments. In contrast with the case of $C_{b,0} = 0.29\%$ without Marangoni effect, it can be inferred from Figure 13 that the Marangoni effect can improve the mass-transfer coefficient in the MIBK–acetic acid–water system because the local sub-drop convection eddies near the interface do promote the interphase mass transfer. There is a substantial difference between the predicted and measured mass-transfer coefficients for Runs 1 and 2. We think that the error may be caused by the larger numerical Marangoni effect induced oscillations in rise velocities as compared with the observed oscillations. The reason of similarity between 7.75% run and 0.29% run after 1.5 s is that the Marangoni effect in 7.75% run dies away after 1.5 s. However, the Marangoni effect of 12.01% run still exists after 1.5 s. The Marangoni effect is very obvious in the initial stage of the mass transfer, typically shorter than 0.1 s. However, it is difficult to measure the mass-transfer coefficient within such short time with the present experimental technique. The numerical

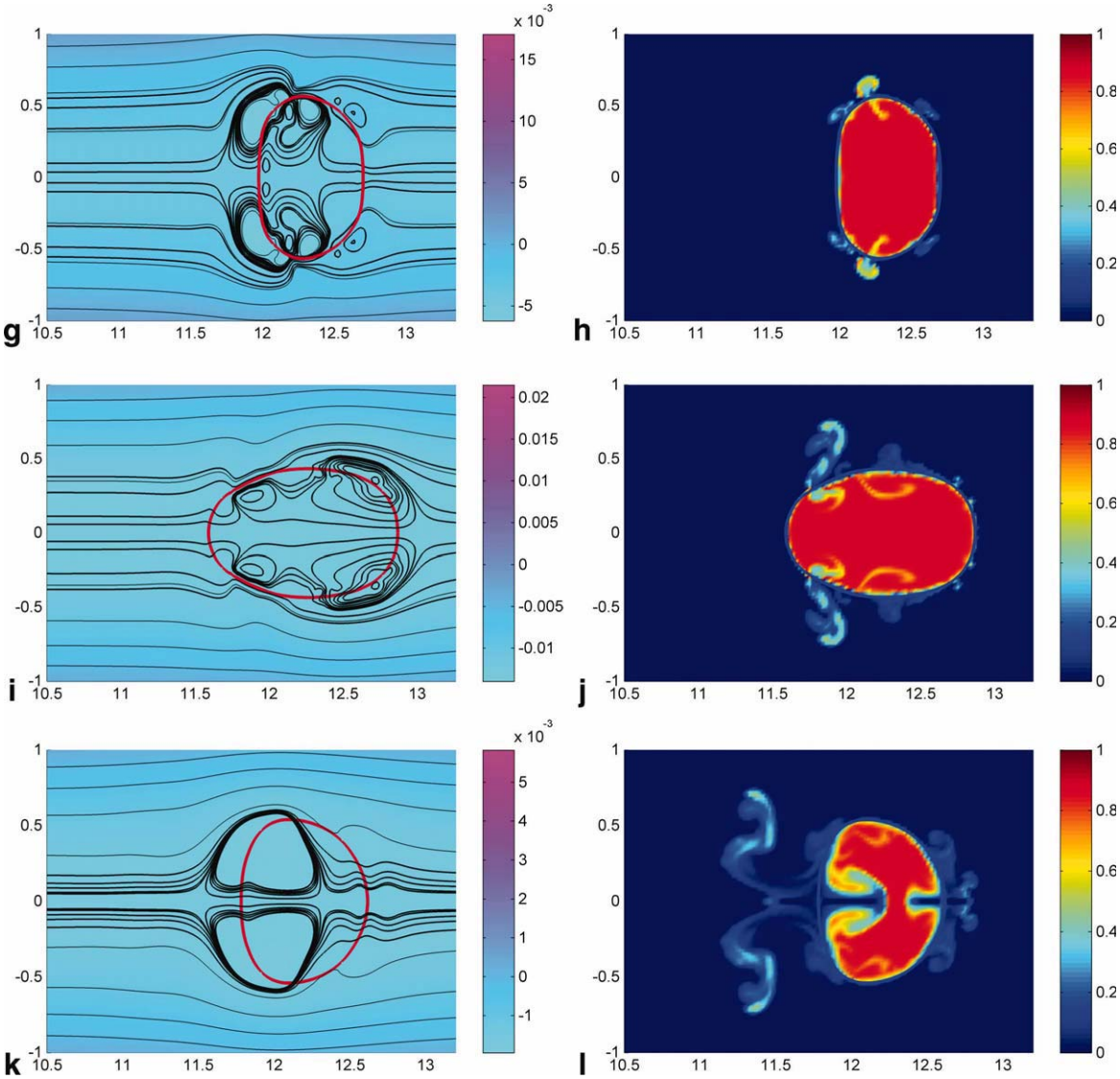

Figure 12. (Continued).

simulation may be a useful tool for this kind of problem, though the quantitative agreement with experimental data is to be pursued in the future.

In Figure 14, we also compare the simulated mass-transfer coefficient of $C_{b,0} = 12.01\%$ for a deformable droplet with that for a spherical one to show the influence of deformation on mass-transfer coefficient. The mass-transfer coefficients of simulation considering the deformation are closer to the experimental measurements, namely, the prediction error of simulation for a spherical drop is larger than that for a deforming drop. This suggests that it is necessary to take the drop deformation into the consideration for realistic numerical simulation.

Conclusions

Experimental determination and numerical simulation of the interphase mass transfer from a deformable drop moving in a continuous immiscible liquid in the laminar flow regime under the influence of Marangoni effect are presented in this article. Three experiments in the MIBK–acetic acid–water system, which has a nonlinear relationship between the interfacial tension and the solute concentration, with different initial drop concentrations were simulated by a level set approach, and the numerical results agree generally with the experimental data.

The predicted final velocity of a rising drop with and without Marangoni convection is in agreement with the experimental. The mass-transfer coefficient of the cases with Marangoni effect is larger than that without Marangoni effect, which sheds a light to manipulating the Marangoni effect to enhance mass-transfer coefficients in extraction processes. It is found when the Marangoni effect is stronger, the oscillation of the drop rising velocity is also stronger and the mass-transfer coefficient becomes larger. Numerical simulations depict well the transient flow structure of the Marangoni effect induced by interphase mass transfer and suggest that stronger Marangoni effect will deform the drop interface in a more irregular way. In all cases, the drop will finally resume its ellipsoidal shape for the steady motion when the Marangoni effect dies away gradually.

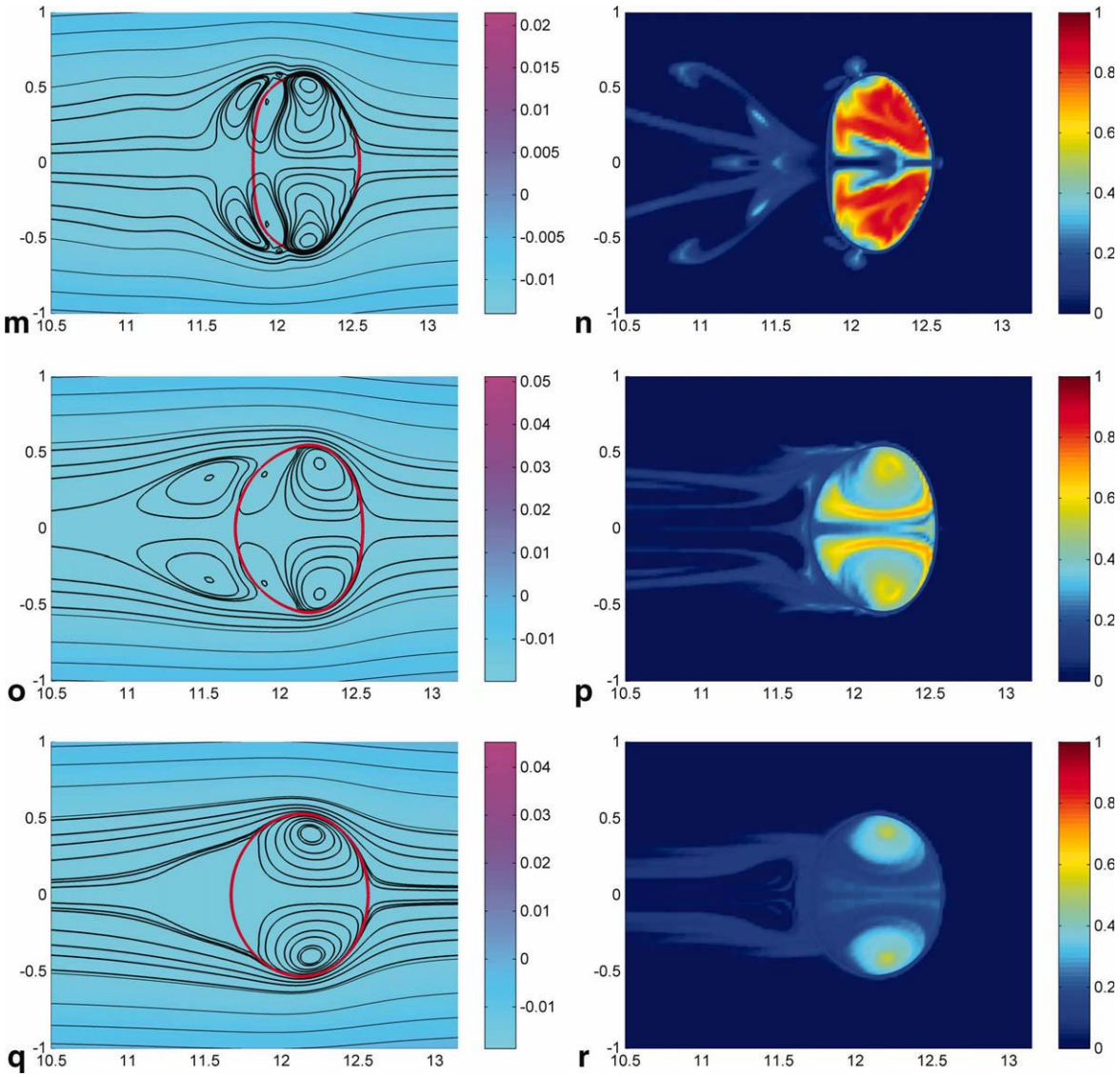

Figure 12. (Continued).

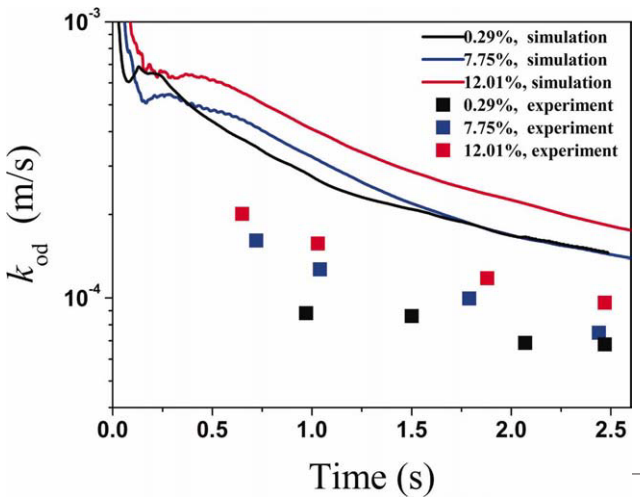

Figure 13. Influence of Marangoni effect on mass-transfer coefficient.

[Color figure can be viewed in the online issue, which is available at wileyonlinelibrary.com.]

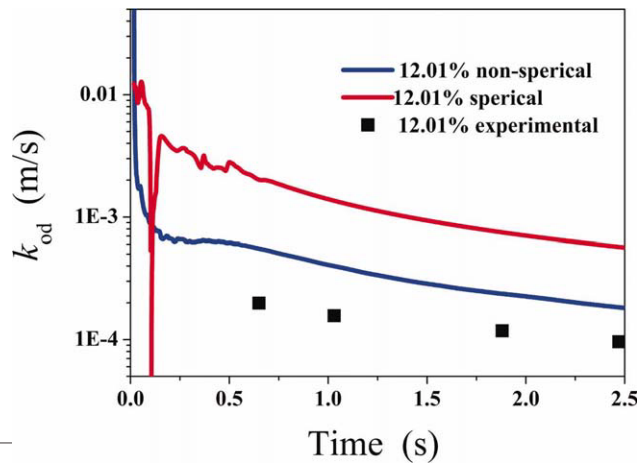

Figure 14. Influence of deformation on mass-transfer coefficient.

[Color figure can be viewed in the online issue, which is available at wileyonlinelibrary.com.]

The predictions of mass-transfer coefficients are qualitatively in accord with the experimental measurements. The reason of the difference between the numerical and experimental results is probably that the Marangoni effect is 3-D in nature and the interfacial eddies on the sub-drop scale would not be in the toroidal form, which is prescribed *a priori* by the axisymmetrical coordinate system. In fact, quantitative prediction of the measured mass transfer with Marangoni effect is rather difficult due to many factors including the pulsation of drop shape and oscillation of rise velocity. These asymmetric features of fluid flow influence the interphase mass transfer on a large extent, but they cannot be well accounted for in the frame of 2-D simulation. It is strongly felt that 3-D phenomena are possibly described reasonably well only with the 3-D simulation using the numerical procedure further improved with higher efficiency and accuracy.

Acknowledgments

Financial support from the National Natural Science Foundation of China (Nos. 20990224 and 20906090), the National Science Fund for Distinguished Young Scholars (21025627), 973 Program (2009CB623406), 863 Project (2007AA060904), and the Jiangsu Province Projects (BY2009133 and BE2008086) are gratefully acknowledged.

Notation

C = concentration, wt %
C^* = concentration in equilibrium with other phase, wt %
C_1^s = dimensionless concentration ($C/C_{b,0}$)
D = molecular diffusivity of solute, m^2/s
$\mathbf{F}_{Ma}$ = Marangoni force, N/m^3
Fr = Froude number, $U^2/(2Rg)$
g = acceleration vector of gravity, m/s^2
h = mesh size
k_{od} = overall mass-transfer coefficient, m/s
m = distribution coefficient
$\mathbf{n}$ = unit vector normal to surface
P = pressure, Pa
Pe = Peclet number, $Pe = 2RU/D_1$
r = radial coordinate, m
R = radius of drop, m
Sh = Sherwood number, $2Rk_{od}/D$
τ = stress tension, N/m^2
t = time, s
U = terminal velocity, m/s
$\mathbf{u}$ = velocity vector, m/s
u = axial velocity component, m/s
v = radial or transverse velocity component, m/s
We = Weber number, $2\rho_1 U^2 R/\sigma_0$
x = axial coordinate, m
y = radial or transverse coordinate, m
ϕ = level set function, m
μ = viscosity, Pa/s^{-1}
ρ = density, kg/m^3
σ = surface tension, N/m
σ_0 = surface tension of pure system, N/m

Subscripts

1, c = continuous phase
2, b = drop
in = first measurement location
out = second measurement location
∞ = remote boundary
s = interface

Literature Cited

1. Sternling CV, Scriven LE. Interfacial turbulence: hydrodynamic instability and the Marangoni effect. *AIChE J*. 1959;5:514–523.
2. Pearson JRA. On convection cells induced by surface tension. *J Fluid Mech*. 1958;4:489–500.
3. Brian PLT. Effect of Gibbs adsorption on Marangoni instability. *AIChE J*. 1971;17:765–772.
4. Scanlon JW, Segel LAJ. Finite amplitude cellular convection induced by surface tension. *J Fluid Mech*. 1967;30:149–162.
5. Cloot A, Lebon G. A nonlinear stability analysis of the Benard-Marangoni problem. *J Fluid Mech*. 1984;145:447–469.
6. Golovin AA, Nepomnyashchy AA, Pismen LM. Pattern formation in large-scale Marangoni convection with deformable interface. *Physica D*. 1995;81:117–147.
7. Bragard J, Slavtchev SG, Lebon G. Nonlinear solutal Marangoni instability in a liquid layer with an adsorbing upper surface. *J Colloid Interface Sci*. 1994;168:402–413.
8. Okano Y, Fukuda T, Hirata A, Takano N, Tsukuda T, Hozawa M, Imaishi N. Numerical study on Czochralski growth of oxide single crystals. *J Cryst Growth*. 1991;109:94–98.
9. Kobayashi M, Tsukuda T, Hozawa M. Effect of internal radiative heat transfer on the convection in CZ oxide melt. *J Cryst Growth*. 1997;180:157–166.
10. Gałązka Z, Wilke H. Influence of Marangoni convection on the flow pattern in the melt during growth of $Y_3Al_5O_{12}$ single crystals by the Czochralski method. *J Cryst Growth*. 2000;216:389–398.
11. Kawaji M, Gamache O, Hwang DH, Ichikawa N, Viola JP, Sygusch J. Investigation of Marangoni and natural convection during protein crystal growth. *J Cryst Growth*. 2003;258:420–430.
12. Braescu L, Duffar T. Effect of buoyancy and Marangoni forces on the dopant distribution in a single crystal fiber grown from the melt by edge-defined film-fed growth (EFG) method. *J Cryst Growth*. 2008;310:484–489.
13. Bergeron A, Henry D, Benhadid H. Marangoni-Bénard instability in microgravity conditions with Soret effect. *Int J Heat Mass Transf*. 1994;37:1545–1562.
14. Bergeron A, Henry D, Benhadid H, Tuckerman LS. Marangoni convection in binary mixtures with Soret effect. *J Fluid Mech*. 1998;375:143–177.
15. Bahloul A, Delahaye R, Vasseur P, Robillard L. Effect of surface tension on convection in a binary fluid layer under a zero gravity environment. *Int J Heat Mass Transf*. 2003;46:1759–1771.
16. Lappa M, Piccolo C, Carotenuto L. Mixed buoyant-Marangoni convection due to dissolution of a droplet in a liquid–liquid system with miscibility gap. *Eur J Mech B Fluids*. 2004;23:781–794.
17. Kang YT, Kashiwagi T. Heat transfer enhancement by Marangoni convection in the NH_3–H_2O absorption process. *Int J Refrig*. 2002;25:780–788.
18. Kim J, Kang YT, Choi CK. Effects of gas phase and additive properties on Marangoni instability for absorption process in a horizontal fluid layer. *Int J Refrig*. 2004;27:140–149.
19. Kim J, Choi CK, Kang YT. Instability analysis of Marangoni convection for absorption process accompanied by heat transfer. *Int J Heat Mass Transf*. 2004;47:2395–2402.
20. Bassano E. Numerical simulation of thermo-solutal-capillary migration of a dissolving drop in a cavity. *Int J Numer Methods Fluids*. 2003;41:765–788.
21. Mao Z-S, Chen JY. Numerical simulation of the Marangoni effect on mass transfer to single slowly moving drops in the liquid–liquid system. *Chem Eng Sci*. 2004;59:1815–1828.
22. Wang JF, Yang C, Mao Z-S. Numerical simulation of Marangoni effects of single drops induced by interphase mass transfer in liquid-liquid extraction systems by the level set method. *Sci China B: Chem*. 2008;51:684–694.
23. Mao Z-S, Lu P, Zhang GJ, Yang C. Numerical simulation of the Marangoni effect with interphase mass transfer between two planar liquid Layers. *Chin J Chem Eng*. 2008;16:161–170.
24. Wegener M, Eppinger P, Baumler K, Kraume M, Paschedag AR, Bansch E. Transient rise velocity and mass transfer of a single drop with interfacial instabilities—numerical investigations. *Chem Eng Sci*. 2009;64:4835–4845.
25. Harlow FH, Welch JE. Numerical calculation of time-dependent viscous incompressible flow of fluid with free surface. *Phys Fluids*. 1965;8:2182–2189.
26. Hirt CW, Nichols BD. Volume of fluid (VOF) method for the dynamics of free boundaries. *J Comput Phys*. 1981;39:201–255.

27. Unverdi OS, Tryggvason GJ. A front-tracking method for viscous, incompressible, multi-fluid flows. *J Comput Phys*. 1992; 100:25–37.
28. Baker GR, Moore DW. The rise and distortion of a two-dimensional gas bubble in an inviscid liquid. *Phys Fluids A*. 1989; 1:1451–1459.
29. Osher S, Sethian J. Fronts propagating with curvature-dependent speed: algorithms based on Hamilton-Jacobi formulations. *J Comput Phys*. 1988;79:12–49.
30. Li TW, Mao Z-S, Chen JY. Terminal effect of drop coalescence on single drop mass transfer measurements and its minimization. *Chin J Chem Eng*. 2001;9:204–207.
31. Brackbill JU, Kothe DB, Zemach C. A continuum method for modeling surface tension. *J Comput Phys*. 1992;100:335–354.
32. Wang JF, Yang C, Mao Z-S. A simple weighted integration method for calculating surface tension for suppression of parasitic flow in the level set approach. *Chin J Chem Eng*. 2006;14:740–746.
33. Misek T. *Recommended Systems for Liquid Extraction Studies*. Rugby, U.K.: EPEC Publications Series. Institute of Chemical Engineers, 1978.
34. Yang C, Mao Z-S. An improved level set approach to the simulation of drop and bubble motion. *Chin J Chem Eng*. 2002;10:263–272.
35. Yang C, Mao Z-S. Numerical simulation of interphase mass transfer with the level set approach. *Chem Eng Sci*. 2005;60:2643–2660.
36. Patankar SV. *Numerical Heat Transfer and Fluid Flow*. Washington: Hemisphere, 1980.
37. Van Doormaal JP, Raithby GD. Enhancements of the SIMPLE methods for prediction incompressible fluid flows. *Numer Heat Transf*. 1984;7:147–163.
38. Fedkiw RP, Aslam T, Merriman B, Osher S. A non-oscillatory Eulerian approach to interfaces in multimaterial flows (the ghost fluid method). *J Comput Phys*. 1999;152:457–492.
39. Jiang GS, Shu CW. Efficient implementation of weighted ENO schemes. *J Comput Phys*. 1996;126:202–228.
40. Wang JF, Lu P, Wang ZH, Yang C, Mao Z-S. Numerical simulation of unsteady mass transfer by the level set method. *Chem Eng Sci*. 2008;63:3141–3151.
41. Mao Z-S, Lu P, Zhang GJ, Yang C. Numerical approach to the three-dimensional Marangoni effect in a two liquid layer system. In: *International Solvent Extraction Conference (ISEC'2008)*, Tucson, USA, September, 2008.

Manuscript received Nov. 30, 2009, revision received Aug. 14, 2010, and final revision received Oct. 29, 2010.